

PCCP

Accepted Manuscript



This is an *Accepted Manuscript*, which has been through the Royal Society of Chemistry peer review process and has been accepted for publication.

Accepted Manuscripts are published online shortly after acceptance, before technical editing, formatting and proof reading. Using this free service, authors can make their results available to the community, in citable form, before we publish the edited article. We will replace this *Accepted Manuscript* with the edited and formatted *Advance Article* as soon as it is available.

You can find more information about *Accepted Manuscripts* in the [Information for Authors](#).

Please note that technical editing may introduce minor changes to the text and/or graphics, which may alter content. The journal's standard [Terms & Conditions](#) and the [Ethical guidelines](#) still apply. In no event shall the Royal Society of Chemistry be held responsible for any errors or omissions in this *Accepted Manuscript* or any consequences arising from the use of any information it contains.

Electronic and optical properties of pristine and boron-nitrogen doped graphyne nanotube

B. Bhattacharya, N. B. Singh, R. Mondal and U. Sarkar^{*}

Department of Physics, Assam University, Silchar-788011, INDIA

Abstract

First principle calculations with generalized gradient approximation (GGA) are carried out to analyze electronic and optical properties of armchair and zigzag graphyne nanotube (GNT). Its possible application in optoelectronic devices is also understood. Boron and nitrogen (BN) atoms are doped and the resulting band gap tuning is studied depending on BN substitution site and increasing diameter. The basis of this variation is examined using PDOS, COHP analysis exhibiting a decreasing trend in optical response with an increase in diameter. Reported systems show anisotropic behavior in the low-energy region. Origin of optical responses has been monitored from infrared to UV region depending on the doping site of BN. Due to the large band gap, low reflectivity and low refractive index; BN graphyne nanotubes (BNGNT) have been established to be more suitable systems for novel optoelectronic devices. Owing to strong absorption peaks in the UV region allow them to be better choices for the UV light protection.

^{a)} Author to whom correspondence should be addressed.
Electronic mail: utpalchemiitkgp@yahoo.com (U. Sarkar)

INTRODUCTION

Peculiarity of carbon nanotubes (CNT) and other carbon based materials has drawn an immense attention of the scientific community and it leads to the rapid advancement in the field of electronics.¹⁻⁷ There arise some exciting phenomena like field emission, superconductivity, *etc.*⁸⁻¹⁰ The doped nanomaterials can be used as hydrogen storage materials.¹¹⁻¹³ An extensive research work on the different type of graphene nanotube opens up the possibility of designing a new type of nanotube composed by graphyne having sp and sp^2 hybridized carbon atoms. Graphyne, first predicted by Baughman *et al.*(1987),¹⁴ opened up a new possibility in fabrication of optoelectronic device and many research groups have started using it due to its direct band gap property. Despite their topological similarity to graphene, graphyne has some attractive properties because of the presence of acetylenic group in their structure. Graphyne is mechanically stable¹⁵ and has higher carrier mobility¹⁶ than graphene.¹⁷ Due to diverse types of graphyne, various quasi one dimensional structures (quasi-1D), formed from graphyne, are expected. It is assumed that this diversity in quasi-1D structure together with acetylenic linkage provides a rich variety in optical and electronic properties different from those of ordinary carbon nanotubes. Since γ - graphyne is predicted to be more stable than all other graphynes, we have confined our present study on nanotubes generated from γ - graphyne. At present there are fewer investigations on graphyne nanotube (GNT). In the last few years, the electronic structure of graphyne based nanotube has been predicted by many groups.¹⁸⁻²¹ The band gap modulation of γ - GNTs by applying strain has been reported by Coluci *et al*¹⁸ where they have shown that the band gap of γ - GNTs are independent of tube diameter and chirality. Further work of Wang *et al*²¹ on γ - GNTs discarded the claim that the band gap of γ - GNTs are independent of tube diameter. The band gap and thermo electric figure of merit (ZT) show damped oscillation with tube diameter.²¹ So it paves the way to control the thermoelectric properties of GNTs. Moreover, recent investigation shows that, similar to functionalization of CNT and graphyne, calcium decorated GNTs are effective media for hydrogen storage.²² In addition, B/N doping²³ in α -GNT results' in p-type and n-type semiconducting behavior in the α -GNT which enhances their possible use in electronic devices. The GNTs are not yet synthesized, but the successful synthesis of graphdiyne nanotube arrays through an anodic aluminum oxide template²⁴ enhances the possibility of synthesis of GNT structures. Moreover, the recent synthesis of graphyne flakes, graphdiyne films, graphdiyne tubes and many subunits

of graphyne and graphdiyne²⁴⁻²⁸ and their possible application in the field of electronics, photovoltaics, and catalysis²⁹⁻³⁰ makes our investigation of graphyne nanotube more reasonable and realistic.

Optical property of carbon nanomaterials³¹⁻³⁵ has become one of the major topics of current research. A systematic approach to tune the optical responses of the nanomaterial is required for diverse applications, *e.g.* optoelectronics, light energy conversion, UV light protection and artificial photosynthesis, etc. Till now various methods have been attempted to tune the electronic and optical properties of nanomaterial (graphyne, graphene and nanotube) by applying strain, electric field, doping and by inducing vacancy. Even so, the most accepted method of tuning the electronic and optical responses is co-doping by boron and nitrogen. The tailoring of the band gap, reactivity profile and photophysical properties of different molecular species has been achieved by the replacement of one unit of C-C by isoelectronic B-N bond as reported in many experimental studies and calculations.³⁶⁻³⁸ H-BN sheet and BNNT have been proven to be promising materials due to their large band gap. They are suitable for a number of potential applications in polymeric composites, sensors, catalysts molecule-based logic gates, as well as nano- optoelectronic devices. The recent success in the synthesis of hexagonal boron nitride (h-BN) films and their substantial optical band gap³⁹ enhances the opportunity of their possible use in optoelectronics. The large band gap and relatively low dielectric constant of other BN materials indicate the possibility of their application in short wavelength electroluminescent optics.⁴⁰⁻⁴² The successful synthesis of the hexagonal boron nitride single crystal and the experimental support of ultraviolet lasing⁴³ have made them suitable for UV- light emitting devices. A theoretical prediction of strong absorption in wide UV- region for graphyne, graphdiyne, graphyne-3 like boron- nitride sheet also supports the possibility of tuning optical properties by doping with BN.⁴⁴ It is observed that various isostere of BN molecules are found to be biologically active aromatics⁴⁵ and potential candidate for hydrogen storage,^{46,47} organic electronics,⁴⁸ polymer electrolyte membrane fuel cells.⁴⁹ Moreover, the recent synthesis of boron and nitrogen doped SWNT,⁵⁰⁻⁵¹ BN nanocones, BN nanohorns⁵² and their application in optoelectronics also motivated our present study.

Although theoretical investigations show that there are rich variations in the electronic properties of GNT, the trends in the optical properties are not reported yet. Again, the

tailoring of band gap and optical properties are still worth discussing. In this paper, we have demonstrated a systematic way to engineer the band gap as well as optical properties of armchair and zigzag graphyne nanotubes.

MODEL AND METHOD

Density Functional Theory (DFT) and Time Dependent Density Functional Theory (TDDFT) have been considered to be quite successful in demonstrating the electronic and optical properties of different organic and nano systems.⁵³⁻⁵⁴ In our spin polarized calculation we have used density functional theory (DFT) method as implemented in the Siesta package.⁵⁵ We have used GGA approximation with Perdew-Burke-Ernzerhof (PBE) exchange correlation functional. The norm conserving Troullier-Martins pseudopotentials⁵⁶ and DZP basis are used as available in Siesta code. Relaxation was done to set the maximum force on each atom to be smaller than 0.01 eV/Å. The Mesh cut off energy for the grid is taken to be 400 Rydberg and the Brillouin zone is sampled by 1x1x18 k points in the reciprocal space. Moreover, we have considered singlet spin states for this calculation. The optical property calculation is done by using a broadening parameter of 0.30.

We have calculated the optical properties by using the complex dielectric function $\mathcal{E} = \mathcal{E}_1(\omega) + i\mathcal{E}_2(\omega)$, where $\mathcal{E}_1(\omega)$ and $\mathcal{E}_2(\omega)$ represent the real and imaginary parts of the dielectric function respectively. The imaginary part of the dielectric function, due to direct interband transition, can be obtained from Fermi's golden rule as,

$$\mathcal{E}_2(\omega) = \frac{4\pi^2}{\Omega\omega^2} \sum_{i \in VB} \sum_{j \in CB} \sum_k W_k |\rho_{ij}^a|^2 \delta(\mathcal{E}_{kj} - \mathcal{E}_{ki} - \omega) \quad (1)$$

where Ω represents the unit cell volume and ω denotes the photon energy. The dipole transition matrix element ρ_{ij} which is expressed as $\langle k_j | \widehat{p}_\alpha | k_i \rangle$ and can be obtained from self-consistent band structure. From Kramer Kronig transformation, the real part of the dielectric function can be obtained as

$$\mathcal{E}_1(\omega) = 1 + \frac{4}{\pi} P \int_0^\infty d\omega' \frac{\omega' \mathcal{E}_2(\omega')}{\omega'^2 - \omega^2} \quad (2)$$

Knowing the real and imaginary parts of dielectric function, other optical properties such as absorption coefficient $\alpha(\omega)$, optical conductivity $\sigma(\omega)$, reflectivity $R(\omega)$, refractive index $\mu(\omega)$ and energy loss function $L(\omega)$ can be obtained as,

$$\alpha(\omega) = \sqrt{2} \omega \left[\sqrt{\varepsilon_1^2(\omega) + \varepsilon_2^2(\omega)} - \varepsilon_1(\omega) \right]^{1/2} \quad (3)$$

$$\sigma(\omega) = -i \frac{\omega}{4\pi} |\varepsilon(\omega) - 1| \quad (4)$$

$$R(\omega) = \left[\frac{\sqrt{\varepsilon_1(\omega) + i\varepsilon_2(\omega)} - 1}{\sqrt{\varepsilon_1(\omega) + i\varepsilon_2(\omega)} + 1} \right]^2 \quad (5)$$

$$\mu(\omega) = \left[\sqrt{\varepsilon_1^2(\omega) + \varepsilon_2^2(\omega)} + \varepsilon_1(\omega) \right]^2 / \sqrt{2} \quad (6)$$

$$L(\omega) = \varepsilon_2 / [\varepsilon_1^2(\omega) + \varepsilon_2^2(\omega)] \quad (7)$$

RESULTS AND DISCUSSION

The modulation of electronic and optical properties of armchair and zigzag graphene nanotubes (GNTs) is investigated for different diameters and by placing BN at different sites.

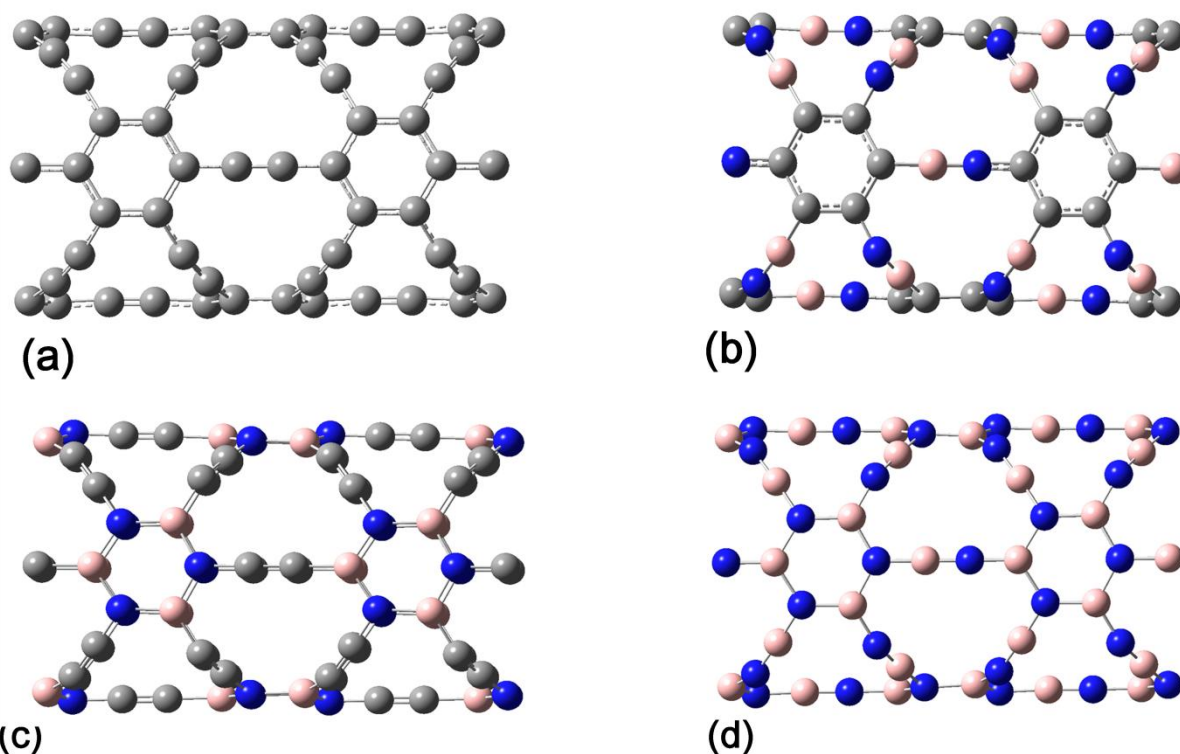


FIG. 1 Geometrical structures of (2,2) graphene nanotube: (a) pristine; (b) graphene with BN at chain; (c) graphene with BN at ring; (d) graphene like BN tube.

We see that all structures retain its non-magnetic behavior due to BN doping at different sites. The optimized structure of (2, 2) zigzag GNT and its BN derivatives are presented in

Fig. 1 and the optimized geometries of (2, 0) GNT with its BN derivatives are provided in supplementary material S1.

Electronic properties:

Bandstructure

The band gap variation of graphyne nanotube as a function of the tube diameter is displayed in Fig. 2. The chirality (or diameter) dependence on band gap variation is clearly visible here for zigzag and armchair nanotubes. Our findings discard the argument that the band gap of graphyne nanotube (GNT) is independent of tube diameter²⁰ and agree with the result obtained by Wang et. al.²¹ More interestingly, a damped oscillation in band gap with tube diameter has been found for pristine GNT, and the band gap converges to that of graphyne sheet with an increasing diameter. We can explain this based on mixing of π and σ orbitals. When the graphyne sheet is rolled-up to form a tube, the orthogonal relation between the σ and π orbitals no longer exists, and the σ and π orbitals mix to stabilize the tube and modify the band structure. For low diameter tube, this mixing becomes larger due to their greater curvature and strain.

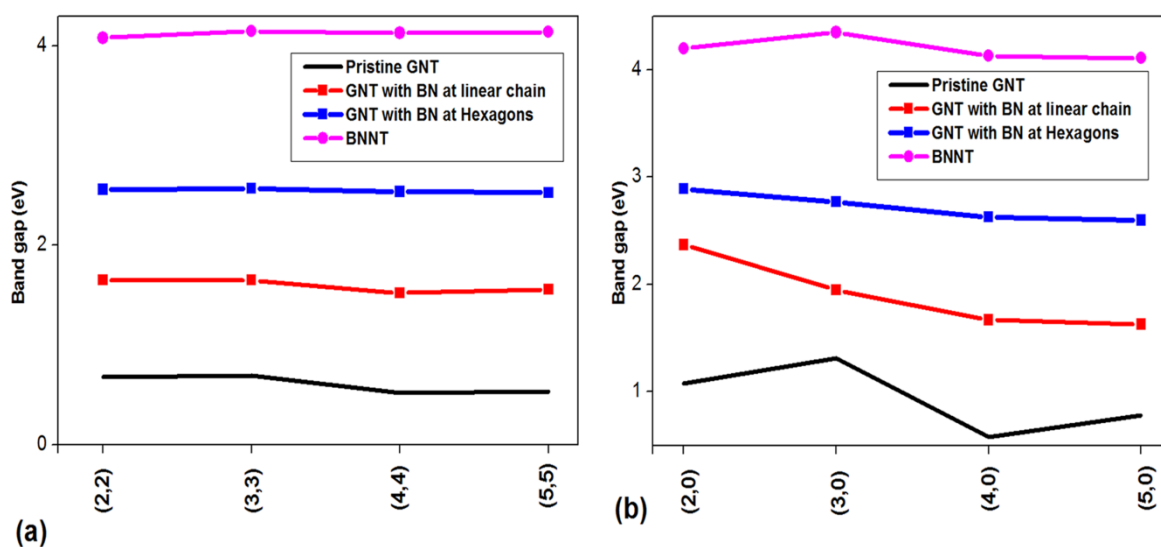


FIG. 2 Variation of band gap with tube diameter and due to BN substitution at different sites; (a) zigzag GNT; (b) armchair GNT.

To design a material for its possible application in electronics and optoelectronics the band gap modification is essential. The presence of boron and nitrogen inserts some impurity states in conduction band (CB) and valence band (VB) respectively, near the Fermi level. Doping by BN at different sites increases the band gap with the trend as pristine system < BN at chain < BN at ring < BN sheet [Fig. 2 and Table S1, S2]. Interestingly, for

zigzag system the BN doping does not affect the damped oscillation of the band gap with increasing tube diameter, but BN doped armchair systems are unable to exhibit damped oscillation with the tube diameter. A decreasing nature of the band gap with an increase in the tube diameter has been observed for armchair GNTs when BN is substituted in linear chain or hexagon. In case of BNGNT the damped oscillation has been observed clearly as we move from (2, 0) to (4, 0) but in case of (5, 0) the oscillation is not prominent. When BN is substituted in the pristine armchair tube, the symmetry of sp^2 / sp -bonded C atoms is broken, as a result of which the damped oscillation disappeared. So, unlike BNNT⁵⁷⁻⁵⁸ it can be assumed that for BN doped armchair GNT the gap can be controlled by chirality as well as chemical composition. Moreover, among all the structures, the band gap is highest for BNGNT and these values range from 4.35 eV to 4.11 eV for armchair BNGNT and 4.08 eV to 4.15 eV for zigzag BNGNT. Our observed values of band gap for BNGNT are comparable to reported value of 2D graphyne like BN sheet (4.20 eV) and BNNT (5.5 eV).

The calculated spin polarized band diagram for pristine and BN doped (2, 2) and (2, 0) GNTs are shown in Fig. 3 where Fig. 3I (b-d) and II (b-d) present the structure with BN at different sites. Here the band for both spins merged together, because the total magnetic moment (due to up spin-down spin) for these systems is zero. As illustrated in Fig. 3, all these novel structures are direct band gap semiconductors except (2,2) zigzag GNT with BN at ring and (2,2) BNGNT.

Our density functional calculation shows that the band gaps are 0.68 eV and 1.08 eV for pristine (2,2) and (2,0) GNT respectively and occur at X point in the Brillouin zone. For a given n , the band gap is greater for armchair GNT in comparison to that in zigzag GNT. Additionally, the band gap location is characterized by the chirality (n) and it is located at X point or Gamma point, depending on whether n is even or odd for pristine GNT (both zigzag and armchair) [Table S1 and S2]. But the presence of BN on these fundamental structures does not follow the above role in all cases. The doping site as well as chirality plays an important role in deciding the band gap location [Table S1 and S2]. As observed from Figs. 3I (b-d) and II (b-d), the band structure around the Fermi energy is significantly affected due to the influence of boron and nitrogen doping with an increase in band gap due to doping at different sites and there is no spin splitting. We found a major change in semiconducting nature of these fundamental structures due to the combination of chirality and varying doping site of BN [Table S1 and S2].

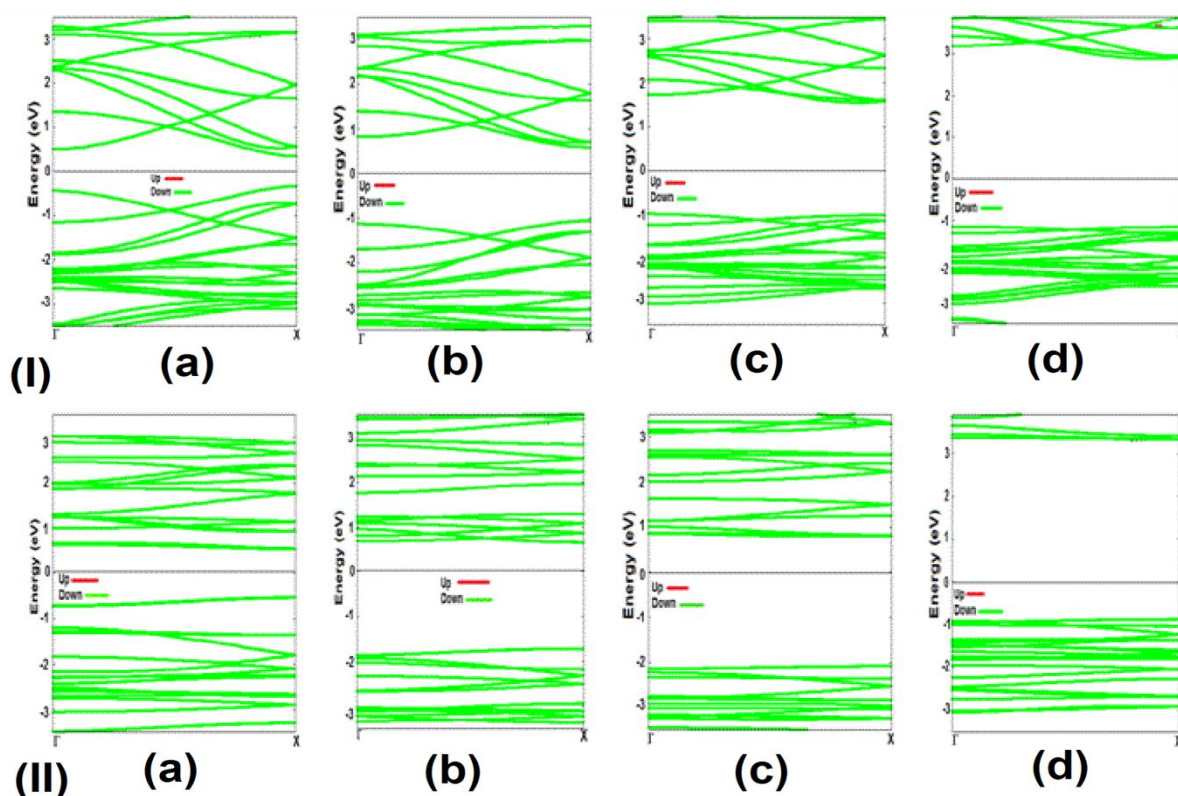


FIG. 3 Band structures for pristine GNT with BN at different sites: (I) (2,2): (a) pristine;(b) BN at chain (c) BN at ring (d) BNNT; (II) (2,0): (a) pristine;(b) BN at chain (c) BN at ring (d) BNNT.

Unlike BN doped graphyne sheet,⁵⁹ in this case the BN doping makes the direct band gap pristine systems as indirect band gap systems in some cases. This effect is more pronounced for zigzag GNT ($n=m$) than armchair GNT ($m=0$). Further; it has been noticed that armchair BNGNTs have a direct and zigzag BNGNTs have an indirect band gap which is consistent with the results found for band structure of armchair and zigzag BNNTs.^{58,60} In case of CNT, armchair is defined by (n,n) and zigzag is defined by $(n,0)$. But, for GNT armchair and zigzag are characterized by $(n,0)$ and (n,n) respectively. So, our armchair BNGNT results should mimic the results of zigzag BNNT.

Partial Density of States (PDOS) analysis

To get a clear idea about the contribution of each constituent orbital we have presented spin polarized projected density of states along with total density of states of pristine and BN doped (2,2) GNTs in Fig. 4. The PDOS for both spin is symmetric; hence our systems are non-magnetic in nature. Because of the quantum confinement, the nature of PDOS in the 1-D graphyne tube is different from that in 2-D graphyne sheet. In case of graphyne sheet the energy states near the Fermi level is mainly contributed by p_z orbital of carbon atom⁵⁹ while

in case of graphyne tube the energy states near the Fermi level is contributed by p_x and p_y orbitals equally. This difference in PDOS in graphyne and graphyne nanotubes can be explained in terms of curvature of nanotube. For graphyne nanotube, the $2p$ orbitals of carbon atoms can be divided into two categories: the p_z orbital oriented itself along the tube axis (z - axis) and the p_x and p_y aligned themselves as radial components, *i.e.* x and y are taken to be mutually perpendicular to the tube axis. Since the nanotube geometry is not planar, it has some specific curvature depending upon its chirality. As in CNT,⁶¹ this curvature is responsible for the pyramidalization and misalignment of π orbitals between adjacent pairs of conjugated carbon atoms. Due to the pyramidalization some s character is present in the π orbital and distorts the same. Degree of the π orbital misalignment and pyramidalization are inversely proportional to the diameter of tube. The delocalized π bonds are situated symmetrically about the axis of the σ bond. For narrow diameter tube, (2,2) GNT [Fig. 4(a)], the significant contribution of p_z orbital appears at -0.62 eV in the valence band and at 0.46 eV in the conduction band. From PDOS analysis of (3,3), (4,4) and (5,5) GNT [Fig. S2A], it is clear that with increasing diameter the contribution of p_z orbital moves away from the Fermi level as the curvature effect reduces with increasing diameter. The PDOS analysis of armchair nanotube also shows the same behavior [Fig. S2B]. Additionally, like a pristine graphyne sheet, the contribution of carbon atom at linear chain is comparatively greater than that of C- atoms in a hexagon [Fig. 4a (iii)].

The PDOS analysis shows that for both zigzag and armchair BN doped graphyne tubes [Fig. 4(b-d) and Fig. S2C], the top of the valence band and bottom of the conduction band are contributed by p -orbitals of N, B and C atoms. The p orbital of nitrogen primarily contributed at the valence band, affects the top of VB and sweeps the energy states toward lower energy. Similarly, the p orbital of boron mainly contributed to the conduction band affecting the bottom of CB and shifts the energy states towards higher energy, thus widens the band gap by symmetry breaking. The doping by B atom creates impurity states in LUMO, while the HOMO is primarily contributed by negatively charged N. The doping by boron is similar to hole doping, which creates a barrier for electrons that becomes a governing factor. This positive potential helps the density of states to get shifted easily towards the higher-energy side, while the nitrogen doping (same as electron doping) creates a negative potential which pushes the density of states towards the lower energy side that leads to

band gap widening. Our PDOS analysis shows that, the contribution of p_z orbital is negligible near the Fermi level for those bonds which are parallel to the tube axis, but for bonds which are at an angle to the axis the contribution of p_z orbital is very high near the Fermi level. This difference in the contribution of p_z orbital is prominent for $C\equiv C$ or $B\equiv N$ bond and the bond connecting the ring and the chain. However, it is less observed for CC or BN bonds at hexagon.

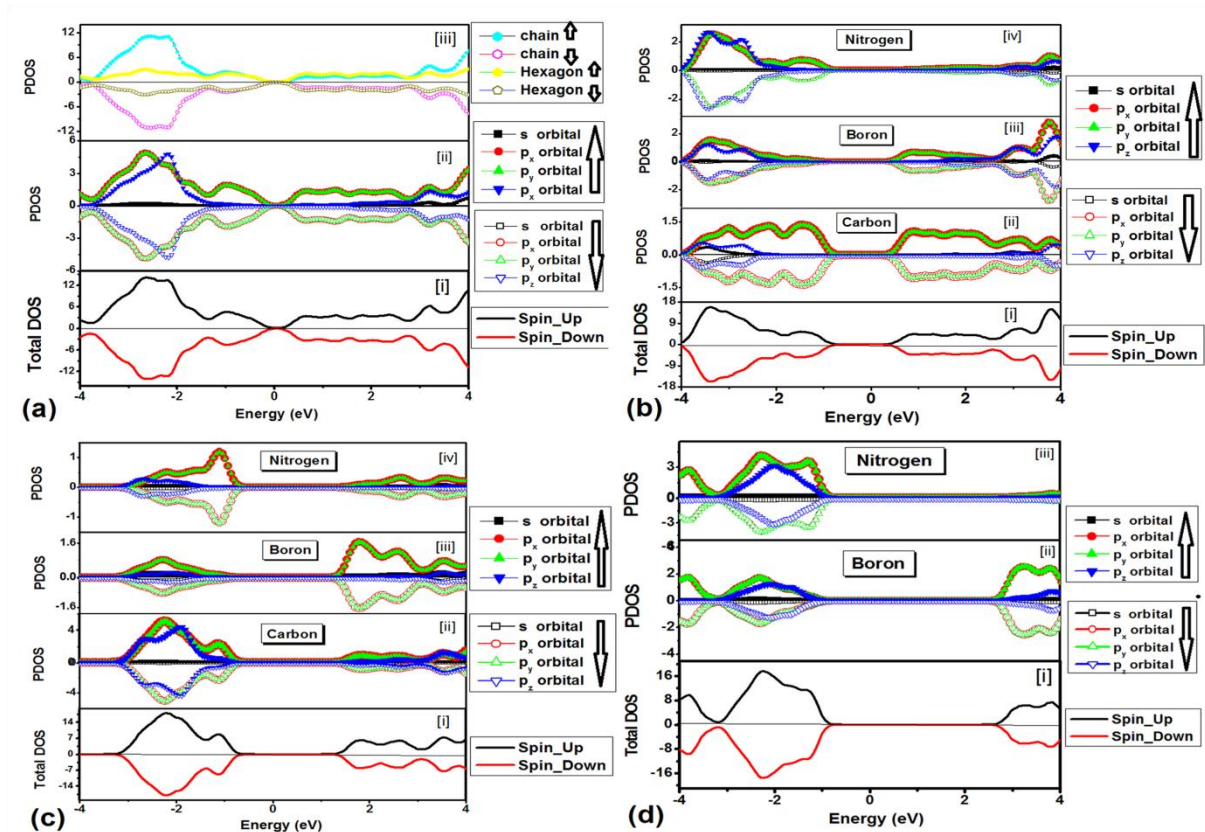


FIG. 4 PDOS analysis of (2,2) GNT: (a) Pristine; (b) BN at chain; (c) BN at ring; (d) BNGNT.

For BNGNT [Fig. 5], there are three types of bonds: BN bond at hexagon having one σ and one dative π bond, BN bond which is connecting ring and chain is having double bond character, and BN bond at chain with one σ , one π and one dative π bond. When we consider the bond parallel to the axis, we see that the VB and CB are mainly contributed by p_y and p_x orbitals of both boron and nitrogen atoms. A small contribution of p_z orbital has been found in BN bond at hexagon. Interestingly, the contribution of BN triple bond is more than BN bond at hexagon and the contribution of BN bond connecting the chain and ring is in between the above mentioned two bonds. Let us consider the bonds, which are at an angle to the axis. Now, a large contribution of p_z orbital has been observed for the boron-

nitrogen triple bond and boron-nitrogen bond connecting ring and chain in VB, but the contribution of p_x gets reduced compared to bond parallel to the tube axis. For boron-nitrogen bond at ring the contribution of p_z and p_y orbitals gets reduced. In pristine GNT, the contribution of orbitals to CC-bonds which are parallel to the tube axis, and at an angle about the axis shows the similar trend as observed in BNGNT [Fig S3]. For bond, parallel to the axis, the σ bonds (contributed by s and p_z) strongly connect the carbon atoms and the π bonds (contributed by p_x and p_y) are perpendicular to the surface of the tube. In this case the π misalignment angle becomes zero. That is why the contribution of p_z axis is not dominant near the Fermi level for those bonds. But for the bonds which are not strictly parallel to the axis, adjacent π orbitals have a non-zero misalignment angle for which the contribution of p_z orbital becomes dominant near the Fermi level in valence band. For BC and NC bonds (in GNT with BN at chain and GNT with BN at ring provided in supplementary material Figs. S4, S5) which are not parallel to the axis, the p_z orbital also contributed at VB near the Fermi level.

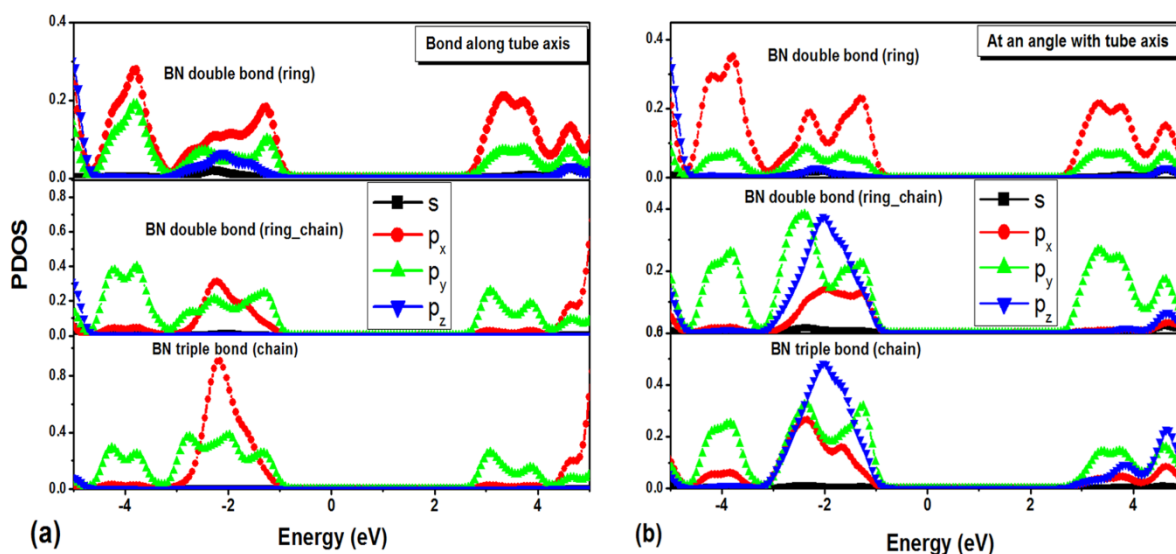


FIG. 5 PDOS analysis of (2, 2) BNGNT in terms of bond: (a) considering the bond parallel to the axis; (b) considering the bond at an angle to the axis.

Charge distribution:

The band gap adjustment of GNT by introducing BN can also be explained through the electron distribution point of view. Fig. 6 presents the charge density plot of (2, 2) GNT. In the pristine system, the charge distribution along the bond is covalent in nature. Due to the

presence of BN the charge is redistributed which in turn changes the corresponding electronic properties. Here the CC bonding exhibits covalent nature due to sharing of electrons between neighboring C-atoms. In the pristine tube [Fig. 6 (a)], the charge is accumulated more near the $\text{-C}\equiv\text{C-}$ bond like pristine graphyne.⁶² Although for both the pristine and BN doped graphyne tube the electron cloud is dispersed all over the system, but the electron cloud is lumpy for BN doped systems due to the accumulation of electron density around the N atom. In the BNC tube the charge transfer occurs mainly from B to N and C to N atoms, hence a net charge accumulation is observed around N atom and a charge depletion is observed around B atom. The accumulation of electrons around N atoms shift the Fermi level towards the conduction band while the depletion of electrons around B atoms causes a shifting of the Fermi level towards the valence band. Hence, the band gap gets widened and this effect is more pronounced in BNGNT.

In BNC derivatives of GNT, BC bond is covalent though it has some ionic character (Fig. 6b and 6c) in which more charge is accumulated near the carbon atom and charge depletion is observed near the boron atom due to the electronegativity difference between carbon and boron atoms. Similarly, some ionic character is observed in NC bond also, though it is covalent in nature, with more charge density located near N atom and less charge density around C atom. Now, the nature of BN bonds depends upon the position where it is substituted. It has been noticed that, when BN is doped at linear chain, the BN bond length is found to be 1.27 Å which is comparable to the BN triple bond ($\text{B}\equiv\text{N}$) in iminoborane (1.252 Å).⁶³ However, when BN is substituted at ring, the BN bond is obtained as 1.47 Å which is in between BN single (B-N) (1.58 Å)⁶⁴ and BN double bonds (B=N) (1.40 Å)⁶⁵ and close to the bond length (1.452 Å) of pristine BNNT. In case of BNGNT, there are three different types of BN bonds, which are situated at: (a) hexagon (1.47 Å) and this bond length is comparable to that of pristine BNNT and borazene (1.44 Å) (b) linear chain (1.27 Å) and (c) the connection between ring and chain (1.40 Å) which is exactly same as BN double bond (B=N) (1.40 Å). Several theoretical studies on BH_3NH_3 , BH_2NH_2 , and HBNH ⁶⁶⁻⁷⁰ approximate the σ and π bond strength of BN bond in terms of bond dissociation energy, heat of formation and atomization energy. It has been noticed that, the Lewis acid-base donor- acceptor σ -bond strength of BH_3NH_3 is comparatively lower than covalent C-C σ -bond strength⁶⁷ of C_2H_6 .

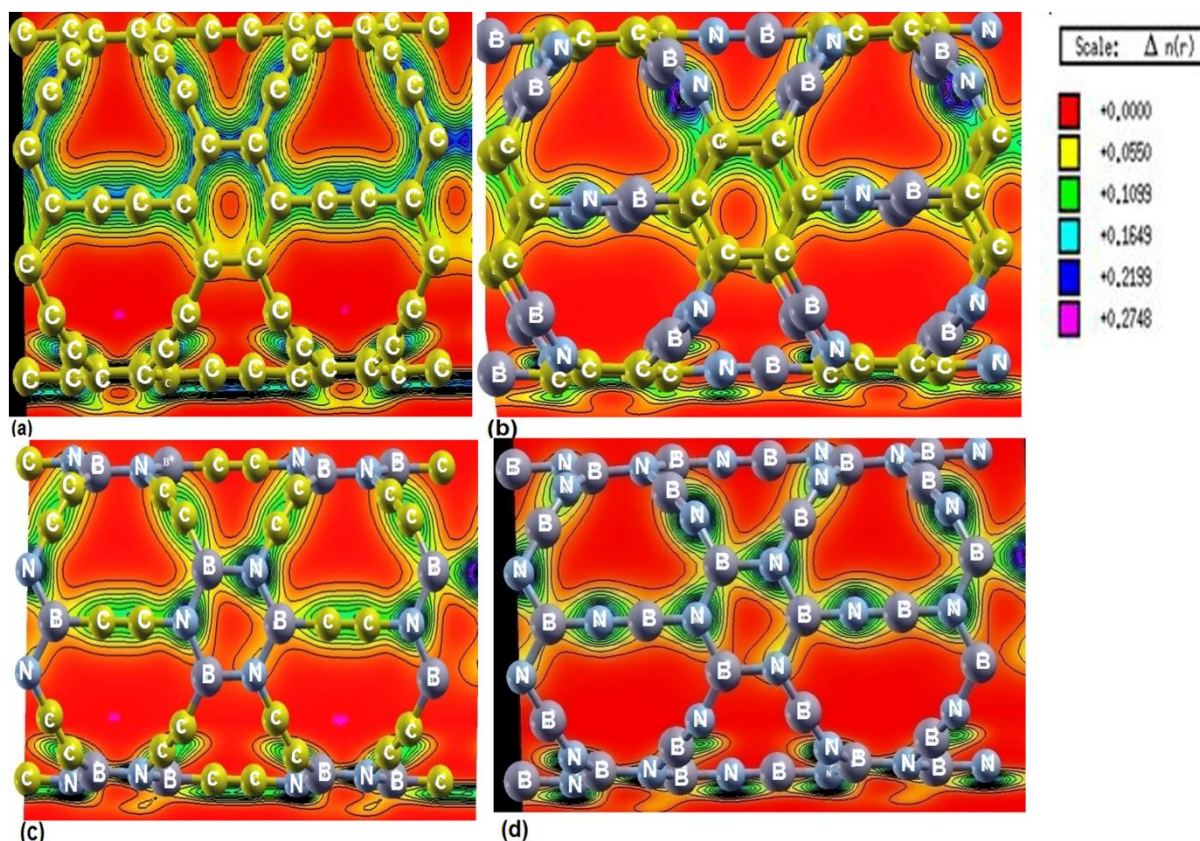


FIG. 6 Charge distribution plot of (2, 2) GNT: (a) pristine; (b) BN at chain; (c) BN at ring; (d) BNGNT.

Grant et al⁶⁷ have given the best estimates of adiabatic σ and π bond strength of aminoborane (BH_2NH_2)⁶⁷ having one σ bond and one dative π bond. The σ bond of BN is comparatively stronger than CC σ bond⁷¹ in ethane with the adiabatic σ -bond strength of 109.8 Kcal/mol and 109.1 Kcal/mol respectively. The π bond of BN is a dative bond and weaker, with comparatively less adiabatic π bond strength (29.9 Kcal/mol), than π bond of CC (65 Kcal/mol). This means, that the adiabatic σ -bond strength of $\text{BH}_2\text{-NH}_2$ ⁶⁷ is comparable to the adiabatic σ -bond strength of ethylene whereas π bond is weaker. The above discussion is consistent with the fact that the bond in BH_2NH_2 includes some ionic character. Similar to aminoborane (BH_2NH_2)⁶⁷ in BNGNT, the BN bond at hexagon, the BN bond connecting chain and ring is in sp^2 environment comprising a mixture of covalent and ionic bonds like in h-BN sheet⁷² containing a weak dative π and a covalent σ bond. For this type (*i.e.* in sp^2 environment) of BN bond,⁷³ nitrogen receives more σ electron density than it gives as π donor from neighboring boron. So the electron density is more localized around the nitrogen atom that results in partial delocalization of charge density, which weakens the π bonding in BN bond in hexagon and bond connecting chain and ring. Since the bond length

of BN at hexagon (1.47 Å) is close to the BN single bond (1.58 Å), it is expected that the BN dative bond at hexagon has some ionic character and it is reflected in Fig. 6. The BN triple bond situated at chain is similar to $\text{HB}\equiv\text{NH}$ (with the total bond dissociation energy 132.0 Kcal/mol at 298 K)⁶⁹. This triple bond consists of a strong σ and two π bonds. The π bonds result from the p orbitals of boron and nitrogen. As B=N bond, the B=N bond at chain also has some ionic character as depicted in Fig. 6(d) due to the presence of dative π bond in it.

-COHP analysis

To support the PDOS study and to highlight the orbital participation in a specific bond, we have presented crystal orbital Hamilton population (-COHP) analysis. In -COHP curves, the positive, negative and zero values point towards bonding, antibonding and non bonding states respectively in a specified energy region.

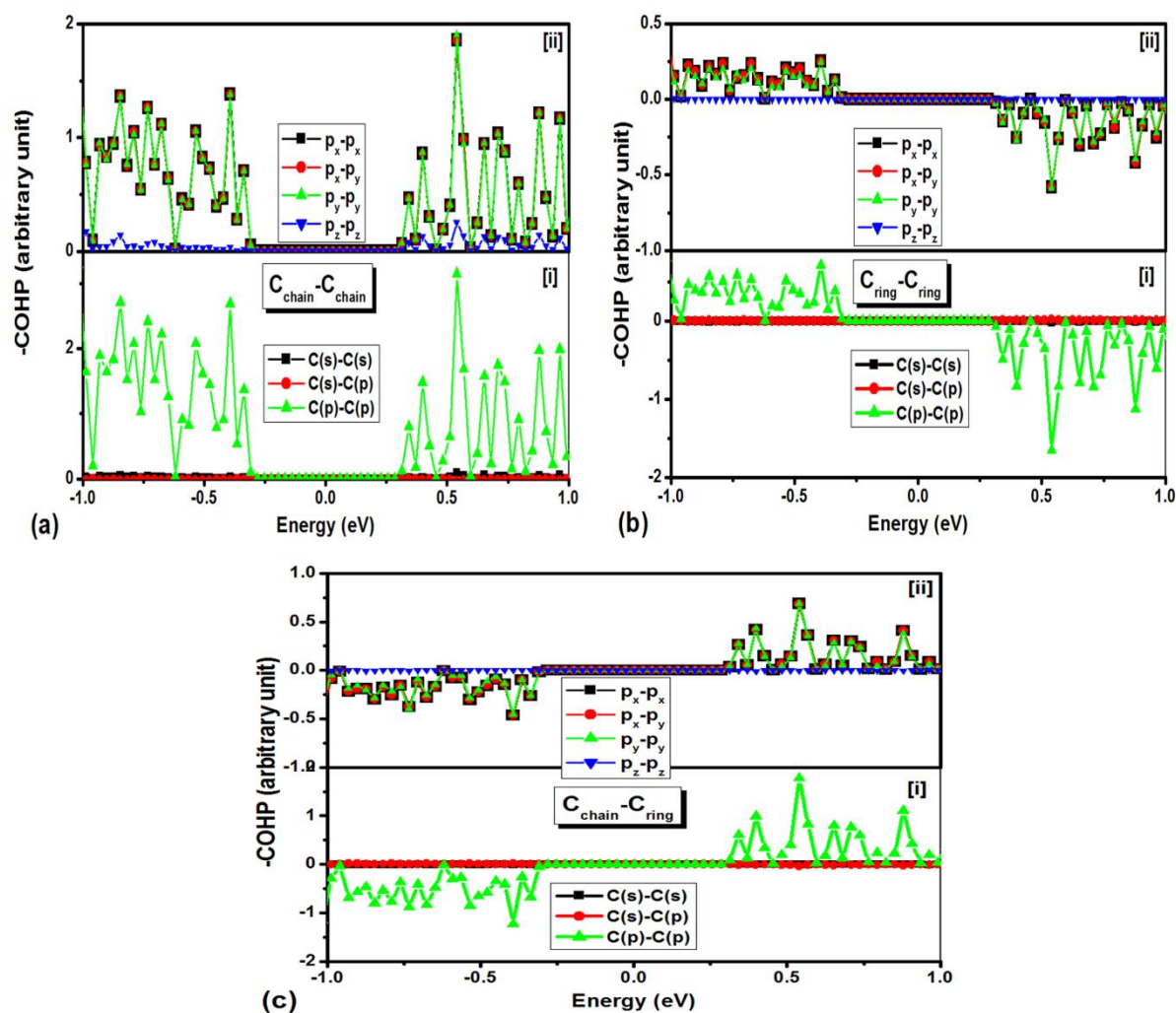


FIG. 7 -COHP analysis of pristine (2,2) GNT; (a) $\text{C}_{\text{chain}}\text{-C}_{\text{chain}}$ (b) $\text{C}_{\text{ring}}\text{-C}_{\text{ring}}$ (c) $\text{C}_{\text{chain}}\text{-C}_{\text{ring}}$

In pristine GNT [Fig. 7], three types of interactions are expected, namely $C_{\text{chain}}-C_{\text{chain}}$, $C_{\text{ring}}-C_{\text{ring}}$ and $C_{\text{chain}}-C_{\text{ring}}$. The C-C interaction of chain gives bonding states near the Fermi level in both valence band and conduction band while the C-C interaction of ring and ring-chain gives both bonding and antibonding states indicating that the $C_{\text{chain}}-C_{\text{chain}}$ bond is stronger than $C_{\text{ring}}-C_{\text{ring}}$ and $C_{\text{chain}}-C_{\text{ring}}$ bonds. The $C_{\text{ring}}-C_{\text{ring}}$ interaction gives bonding states in the valence band and antibonding states in the conduction band but for $C_{\text{chain}}-C_{\text{ring}}$ interaction the opposite trend is observed. The energy states near the Fermi energy are mostly contributed by the *p orbitals* of the nearest neighbor carbon atoms. Close inspection shows that the bonding and antibonding states are mainly contributed by p_x-p_x , p_x-p_y and p_y-p_y orbitals of the carbon atom pair.

Next we consider (2, 2) GNT with BN at chain and the corresponding -COHP curves are depicted in Fig. 8. There are four types of interactions taking place here, namely CC, BC, BN and CN between boron, carbon and nitrogen atoms. The CC interaction reflects the contribution of carbon-carbon bond at hexagon to the total density of states in terms of orbital pair and BN interaction reflects the contribution of boron-nitrogen triple bond at chain. The BC and NC interactions correspond to boron-carbon and nitrogen-carbon bonds respectively, connecting chain and ring. In all these four interactions, the contribution of orbitals participating in bonding and antibonding are provided by p_x-p_x , p_y-p_y and p_x-p_y orbital pairs of neighboring atoms. For CC interaction the p_x-p_x , p_y-p_y and p_x-p_y orbital pairs contribute bonding states at the valence band as well as the conduction band. Same situation prevails for BC interaction where p_x-p_x , p_y-p_y and p_x-p_y orbital pairs of boron-carbon bond contribute antibonding states at VB (some bonding states at -1.7 eV) and bonding states at CB. The NC interaction basically contributes antibonding states at VB and the small presence of bonding states at CB is contributed by p_x-p_x , p_y-p_y and p_x-p_y orbital pairs of neighboring nitrogen and carbon atoms. The BN interaction contributes bonding states at VB and antibonding states at CB arising from p_x-p_x , p_y-p_y and p_x-p_y orbital pairs of boron and nitrogen. For all these above-mentioned interactions the contribution of p_x-p_z , p_y-p_z and p_z-p_z orbital pairs are negligible compared to p_x-p_x , p_y-p_y and p_x-p_y orbital pair contribution. A close inspection shows that, in BN interaction, the p_x-p_z , p_y-p_z and p_z-p_z orbital pairs of boron-nitrogen contribute in VB and CB more significantly than that observed in BC and NC interactions, although this contribution is also small compared to contribution from p_x-p_x , p_y-p_y and p_x-p_y pairs.

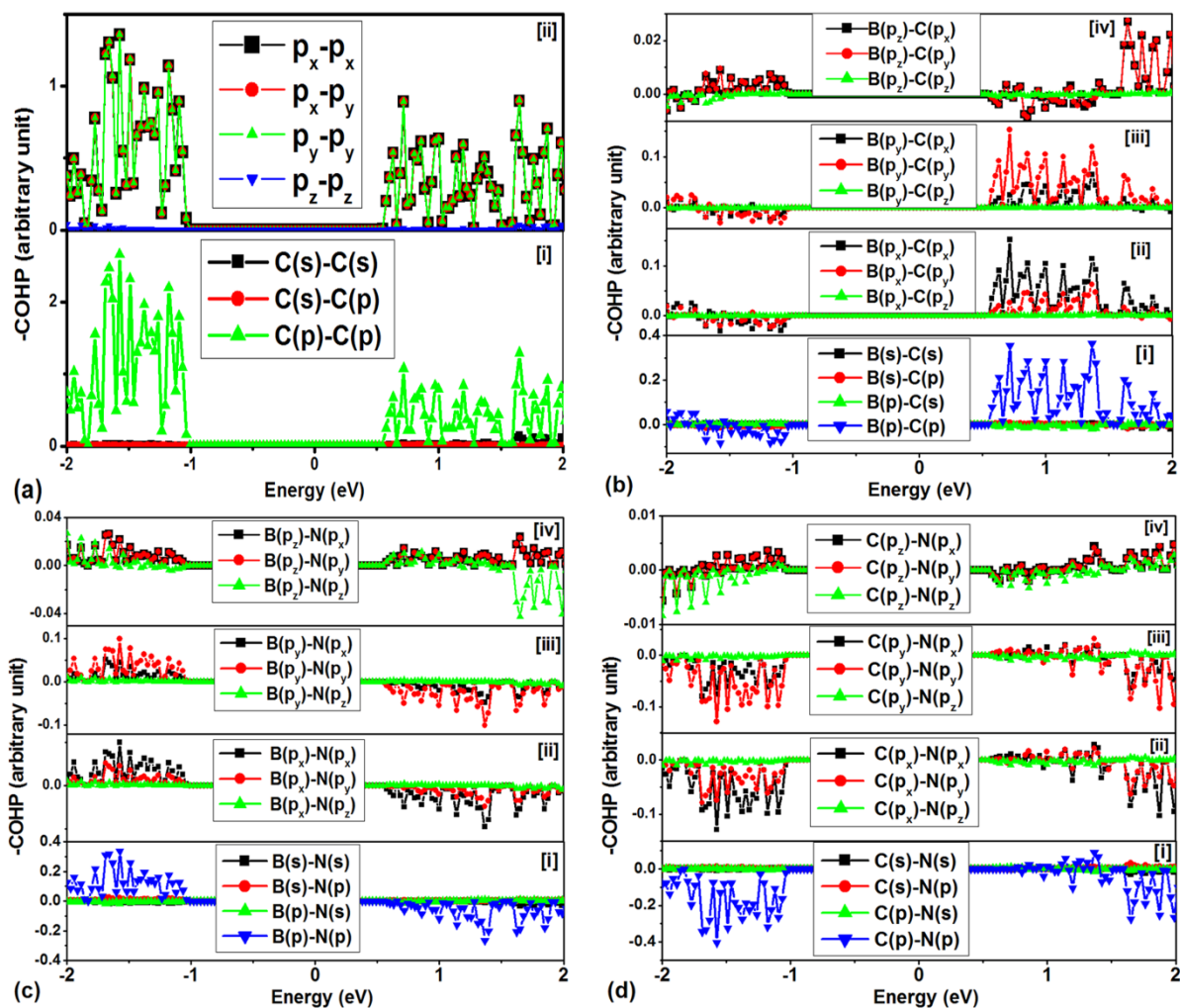


FIG. 8 -COHP analysis of (2,2) GNT with BN at chain considering; (a) C-C; (b) B-C; (c) B-N; (b) C-N interactions.

Now for all these interactions, the bonding/antibonding states arise far away from the Fermi level compared to that in pristine GNT, resulting in an increase in band gap. In these four interactions, it is obvious that the C-C interaction contributes bonding states with a high $-COHP$ value while N-C interaction gives mainly antibonding states, indicating that the C-C interaction is stronger than that in N-C bond.

Next we consider the GNT with BN at ring [Fig. S6]. Here also four types of interactions are present, namely CC, BC, NC and BN. In contrary to GNT with BN at chain here the CC interaction corresponds to the contribution of carbon-carbon triple bond in terms of orbital pairs to the DOS and BN interaction reflects the contribution of boron-nitrogen bond in sp^2 environment to the DOS. The similar situation has been observed for (2, 2) GNT with BN at ring [Fig. S6] but in this case all interactions contain the bonding/antibonding states far away from the Fermi level compared to (2, 2) GNT with BN

at chain. The differences are as follows: (a) the CC interaction contributes more bonding states in VB compared to CB and contribution of p_z-p_z orbital is now significant; (b) in BC interaction, the p_x-p_x , p_y-p_y and p_x-p_y orbital pairs of boron and carbon atom participate in bonding at VB near the Fermi level with larger intensity; (c) for BN interaction, the B(p)-N(s) also participates in bonding along with B(p)-N(p) pair and only B(s)-N(s) contributes antibonding state at -1.8 eV in valence band. However, in CB, only B(p)-N(p) orbital pair contributes. Again in VB, at -1.8 eV, the p_z-p_x , p_z-p_y and p_z-p_z orbital pairs have significant contribution along with p_x-p_x and p_y-p_y orbital pairs. That means in contrary to 'GNT with BN at chain', the contribution of p_z-p_x , p_z-p_y and p_z-p_z orbital pairs become noticeable for 'GNT with BN at ring' although this contribution is small compared to p_x-p_x , p_y-p_y and p_x-p_y orbital pairs.

In case of (2, 2) BNGNT [Fig. S7], there are three types of interactions between neighboring boron–nitrogen atoms. The BN bond at hexagon and BN bond at chain (triple bond) essentially contribute bonding states at the top of the valence band while the BN bond connecting ring and chain contribute antibonding states near the Fermi level in valence band. In CB, the bonding states near the Fermi level is basically contributed by BN bond at hexagon and BN bond connecting ring and chain. The contribution of BN triple bond [Fig. S7] is comparatively larger in top of the VB and contribution of BN bond at hexagon is greater in bottom of CB. We observed that the bonding and antibonding states moved away from the Fermi level, thus resulting in a high increase in band gap. This is due to the enhancement of bonding discrepancy between B and N atoms in BNGNT and the presence of ionic character in B-N bond. Additionally, when we compare the B-N interaction of BNGNT with B-N interaction of (2,2) GNT with 'BN at chain' and (2,2) GNT with 'BN at ring' we found that, in case of GNT with 'BN at chain' and GNT with 'BN at ring' the contribution of p_x-p_x , p_y-p_y and p_z-p_z are less but in BNGNT the contribution of p_x-p_x , p_y-p_y and p_z-p_z orbital pairs of neighboring B and N atom increases.

Optical Properties

The optical properties of armchair and zigzag graphyne nanotube (GNT) with their BNC derivatives and BN analogues are investigated by employing the electric field vector parallel and perpendicular to the tube axis as well as by averaging all directions of propagation of the electric field vector. The first absorption peak of ϵ_2 spectra corresponds

to the band gap between the valence band maxima (VBM) and conduction band minima (CBM) which represent the threshold for direct optical transition and can be treated as optical band gap. We present the ϵ_2 spectra of zigzag GNTs along with its BNC derivatives and BN analogues in Fig. 9, when the electric field is averaged over-all directions. Interestingly, the absorptive part of imaginary dielectric function ϵ_2 is several times larger in low energy region than in high energy region.

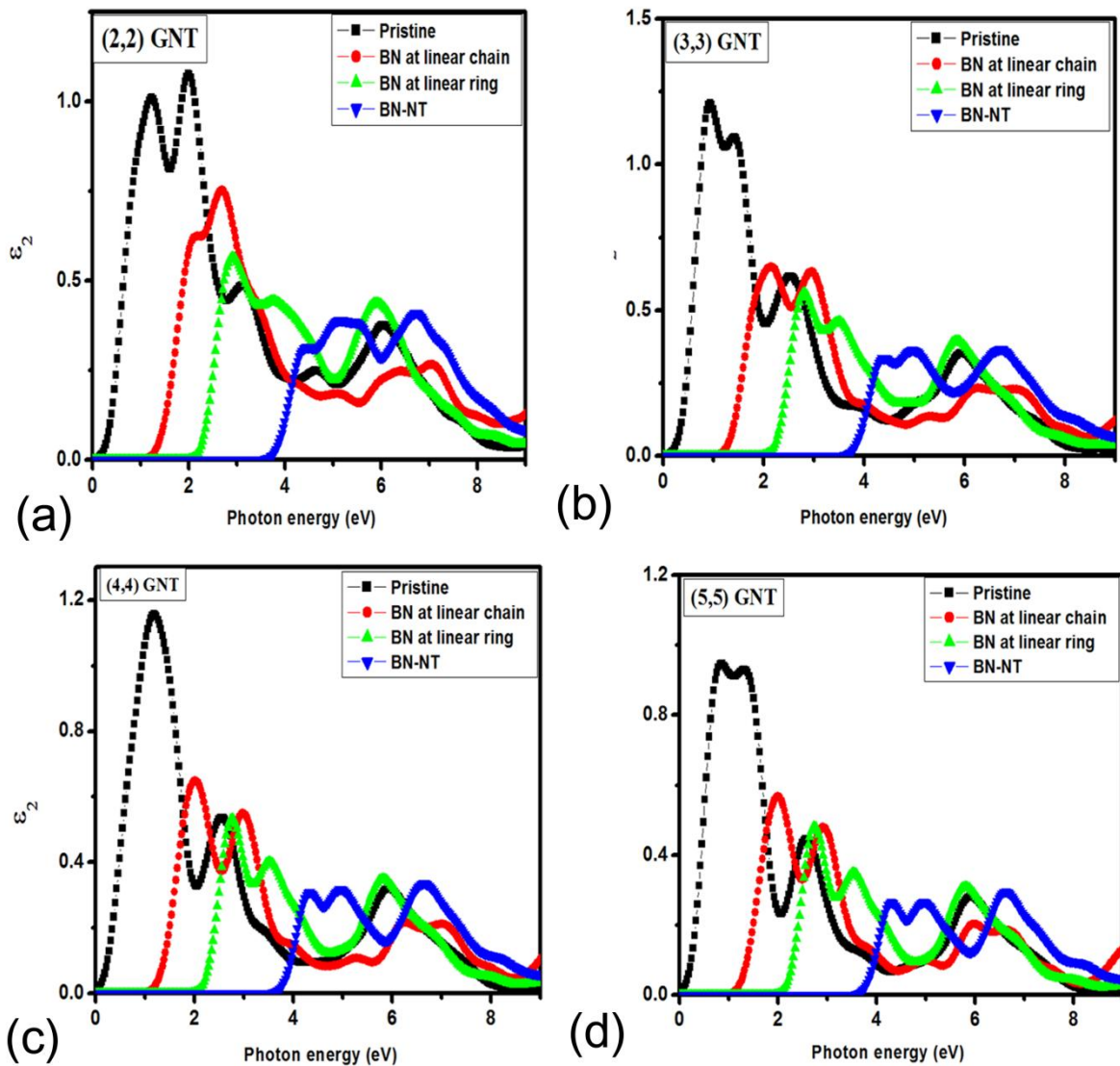


FIG. 9 Variation of first dominant peak of imaginary part of dielectric function with BN at different sites: (a) (2, 2) GNT; (b) (3, 3) GNT; (c) (4, 4) GNT; (d) (5, 5) GNT.

It is clearly visible from Fig. 9 that due to BN doping the first absorption peak gets shifted towards high energy obeying the hierarchy of pristine GNT < GNT with BN at chain < GNT with BN at ring < BNGNT. The intensity decreases with the same trend. We observed

that due to presence of BN the optical band is tuned from infrared region to UV region of electromagnetic spectra depending upon substitution site. More interestingly, the optical band gap lies in infrared region for all pristine tubes; near visible region for graphyne tubes with BN at chain; in visible region for graphyne tubes with BN at ring and in UV region for BNGNTs. The blue shift of strong peak of ϵ_2 absorption spectra due to presence of BN at different sites matches well with UV-*vis* absorption spectra of other BN molecules and BN materials.⁷⁴ The variation in imaginary part of dielectric function (ϵ_2) with tube diameter for zigzag nanotubes [Fig. S8] indicates that the first peak of ϵ_2 spectra follows same trend as the electronic band gap⁷⁵ and the intensity decreases with increasing diameter except in pristine GNT [Fig. S8]. Similar shift of the first peak in ϵ_2 spectra occurs for armchair GNT due to BN doping at different positions [Fig. S9] and the dielectric function decreases in the same fashion as that of the zigzag GNT. We find that dielectric function is the highest for pristine one and the lowest for BNGNT with the highest shift of first peak towards high energy that indicates its large band gap. Because of the high band gap and low dielectric constant of BNGNT, it can be considered as a suitable candidate for short-wavelength optoelectronic device among these fundamental structures.

Next we have considered the parallel and perpendicular polarization. Fig. 10 indicates the real part of dielectric function and Fig. 11 depicts the imaginary part of the dielectric function.

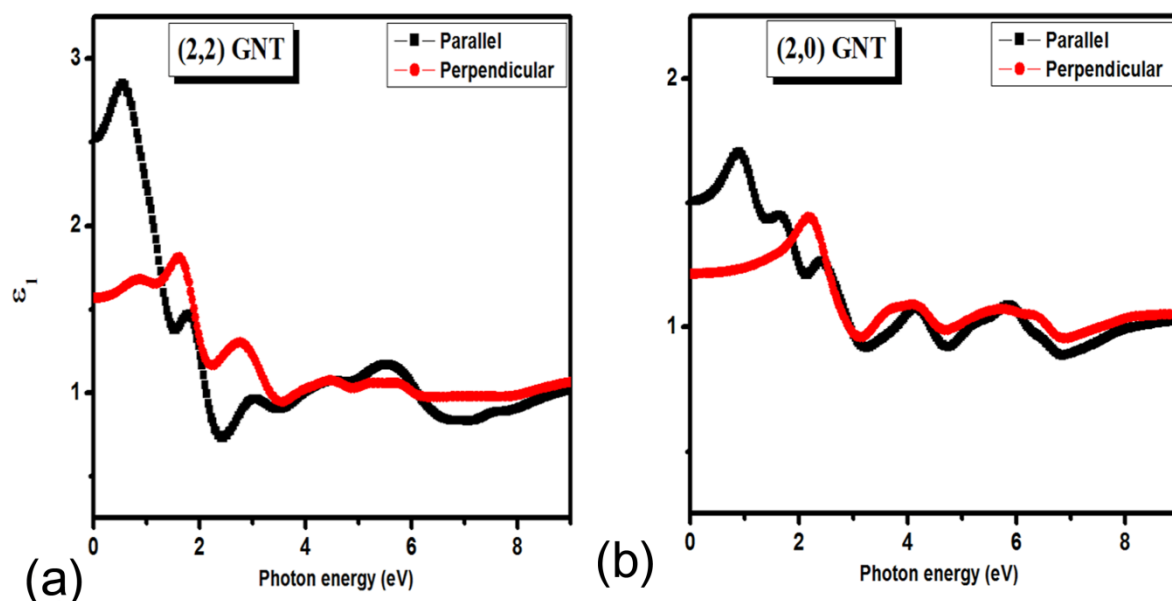


FIG. 10 Variation real part of the dielectric function of pristine: (a) (2, 2) GNT; (b) (2,0) GNT with the incident electric field parallel and perpendicular to the nanotube axis.

Figs. 10(a) and 11(a) represent (2,2) GNT whereas Figs. 10(b) and 11(b) describe (2,0) GNT. For parallel and perpendicular electric fields, the spectra show remarkable anisotropy in the low-energy region.

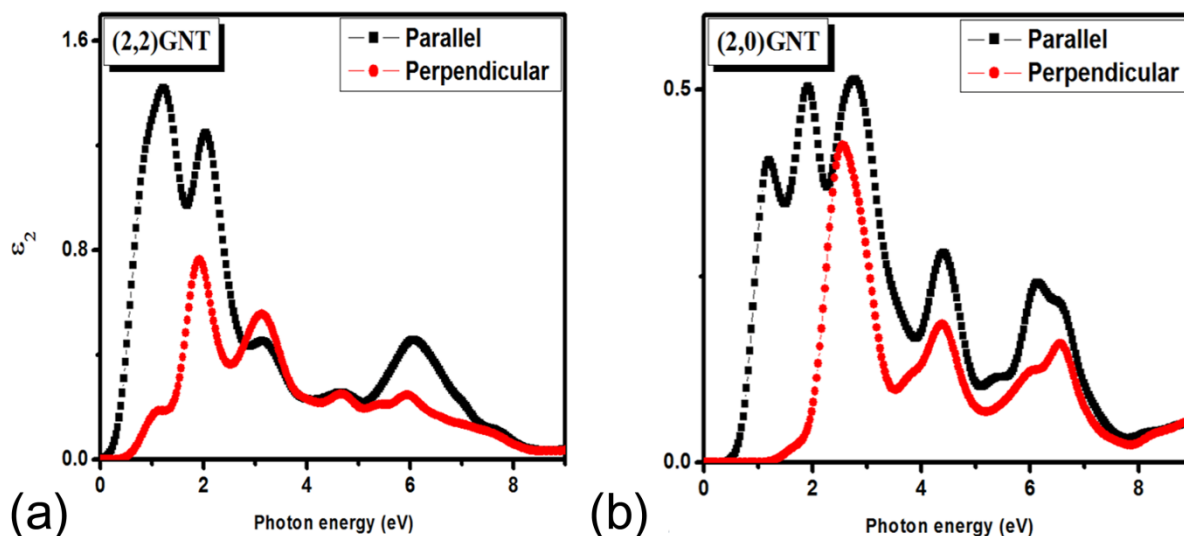


FIG. 11 Variation imaginary part of the dielectric function of pristine: (a) (2, 2) GNT; (b) (2,0) GNT with the incident electric field parallel and perpendicular to the nanotube axis.

The optical anisotropy strongly depends on chirality and diameter. Optical anisotropy decreases with the increase in diameter of the nanotube. We observed that, the imaginary part of the dielectric function for pristine armchair GNT shows much more anisotropy in the very low energy region than for zigzag GNT having same n value [Table S3 and Figs. S10 and S11]. The onset for perpendicular polarization is always higher than the parallel polarization. The comparison of ϵ_2 spectra of GNT with its parent graphyne sheet and ordinary CNT indicates that, in the low energy region, the anisotropy is less prominent for GNT than for graphyne,^{62,76-77} and is similar to that in ordinary CNT.⁷⁸ This is because when a graphyne sheet is rolled up to generate a GNT, the orthogonal relation between π and σ orbitals is getting modified, and they can mix to form a stable GNT. This mixing of π and σ orbitals modifies the electronic structure as well as optical spectra. This gives the evidence that; the optical properties of GNT are mainly dominant by the tubular geometry rather than the flat geometry possessed by its parent sheet structure.

Fig. 12 represents the diameter dependence of absorption spectra of zigzag GNT when electric field is averaged over-all directions of propagation, which provides the information about direction of charge transport and carrier mobility. Clearly, the absorption

coefficient decreases with increasing diameter and the onset of absorption moves towards a high-energy region due to doping by BN at different sites. In case of the pristine system, the absorption starts at infrared region, while for BNGNT the absorption starts at UV region (3.25-3.75 eV). The onset of absorption of systems with BN at chain and BN at ring lies between infrared and UV regions. For systems with BN at ring the absorption starts from UV-vis region (2.23-2.31 eV) and for systems with BN at chain the absorption starts from nearly 1.40-1.6 eV. A similar situation pertains to the absorption spectra of armchair GNT with its BN derivatives [Fig. S12]. Among these structures, only for BNGNT the entire absorption peak appears in quite wide UV region, which indicates the possibility of its use in UV light protection.

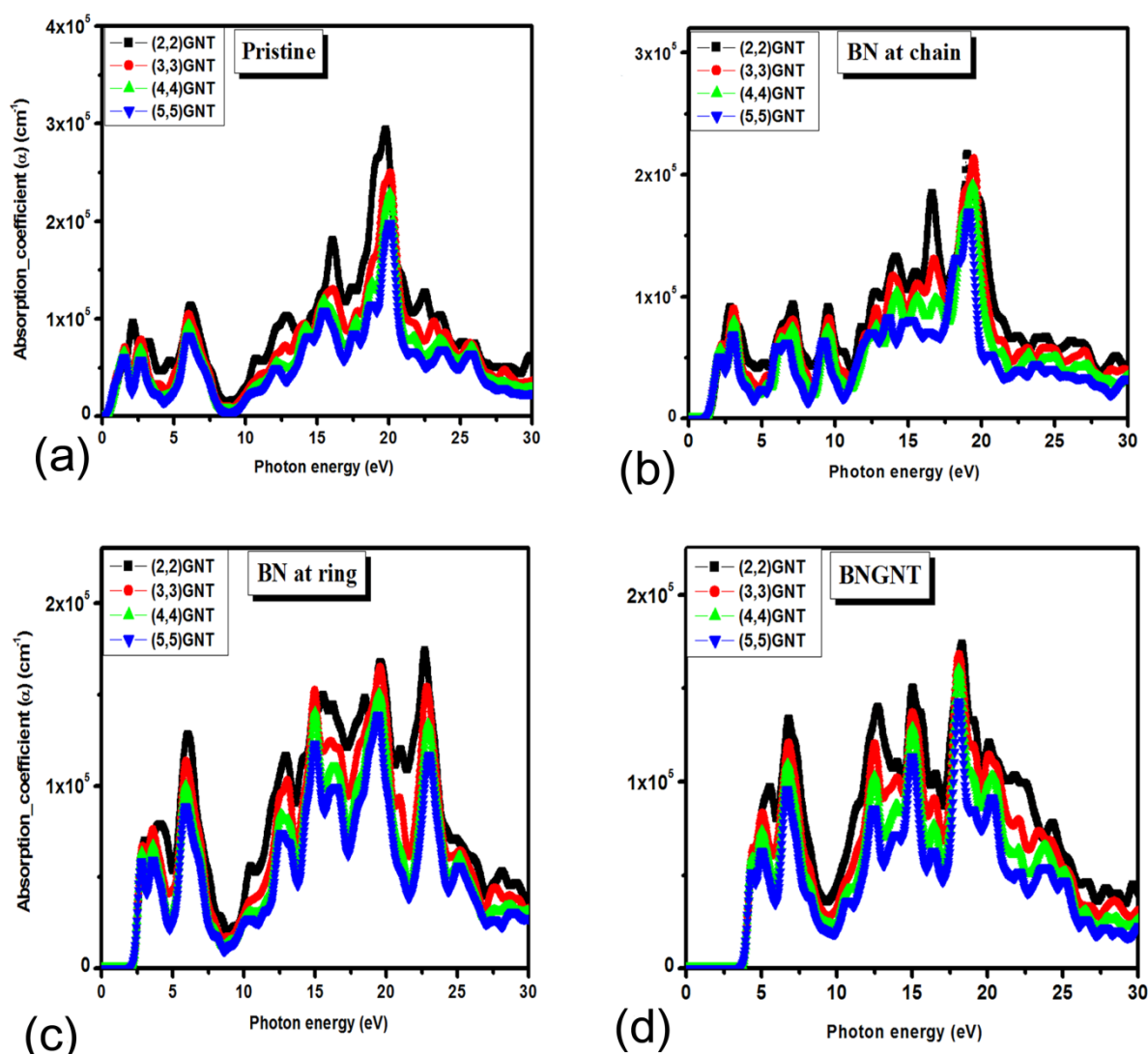


FIG. 12 Diameter dependence of absorption spectra of zigzag graphyne nanotubes: (a) pristine systems; (b) systems with BN at chain; (c) systems with BN at ring; (d) graphyne like BN nanotubes

The absorption spectra of pristine systems with the electric field vector perpendicular to the tube axis and parallel to the tube axis [Fig. S13] show similar nature of absorption. By comparing these three types of absorption spectra (parallel, perpendicular and average polarization) of pristine (2, 0) and (2, 2) GNT [Fig. S14] we can divide the absorption spectra into two regions: namely **A** (0.00-17.50 eV) and **B** (17.50 -30.00 eV). In region **A** the absorption is greater for parallel polarization than perpendicular polarization, but in region **B** the trend is reversed. However, the absorption coefficient for average field is in between the parallel and perpendicular field throughout the energy range.

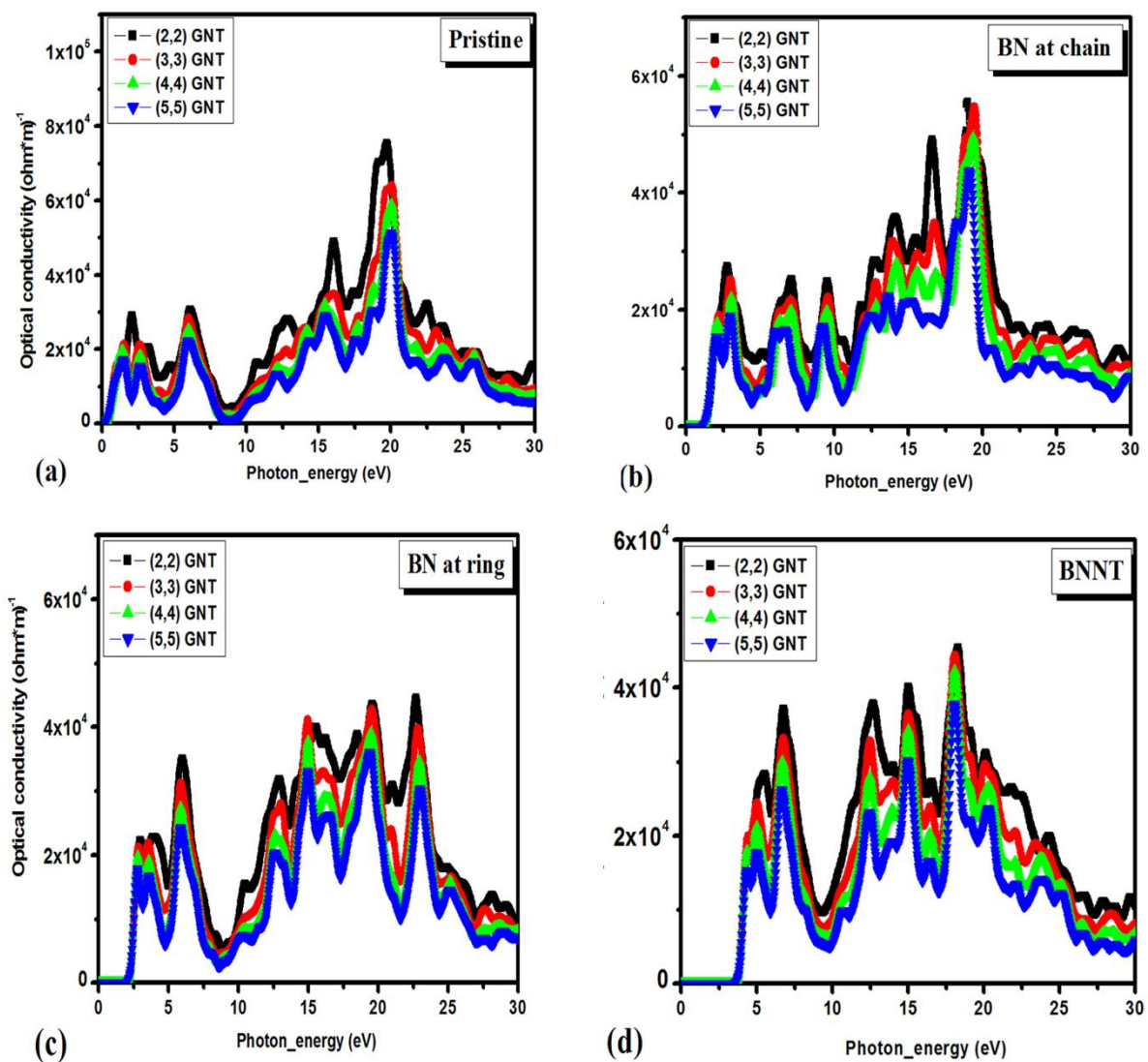


FIG. 13 Diameter dependence of optical conductivity of zigzag graphyne nanotubes: (a) pristine systems; (b) systems with BN at chain; (c) systems with BN at ring; (d) graphyne like BN nanotubes.

The optical conductivity as a function of frequency is presented in Fig. 13 (considering that the electric field is averaged overall directions of propagation). Due to the interaction with electromagnetic radiation the charge in the GNT is redistributed, which in turn affects the optical conductivity of GNT. We see that the optical conductivity decreases with increasing diameter for zigzag GNT including BN at different sites. An identical trend is observed for armchair GNT including BN at different sites [Fig. S15]. The polarization effect on optical conductivity shows the same trend as that in absorption spectra [Fig. S16]. In low-energy region (0.00 – 17.50 eV), for parallel and perpendicular polarizations the optical conductivity is the highest and the lowest respectively. But the opposite trend is found in the high-energy region (17.50 – 30.00 eV). The conductivity of other armchair and zigzag GNTs show similar trends. The first dominant peak of conductivity is shifted towards high energy due to doping by BN [see Table S4 and S5]. This shift not only depends on the type of dopants but also on doping position and concentration obeying the trend of pristine < BN at chain < BN at ring < BNGNT as in their electronic band gap.⁶²

The reflectivity (R) and refractive index (μ) profiles of armchair GNTs are provided in Fig. 14 when electric field is averaged overall directions of propagation. We see that all the structures have low reflectivity and a comparatively high refractive index. This feature is desired in optoelectronic devices such as solar cells and LED.⁷⁹ The reflectivity and refractivity spectra show a gradual decrease in spectral curves with the increase in diameter except the pristine case where the reflectivity and refractivity are greater for (3, 3) GNT. We find that the energy range (0.00- 4.20 eV) is characterized by appreciable values of reflectivity and refractivity. The reflectivity approaches to zero when the energy exceeds by 4.20 eV for the all pristine GNTs. Armchair structures also exhibit the same type of reflectivity and refractivity spectra [Fig. S17]. The strong peaks of reflectivity and refractivity show a blue shift following the trend: pristine < BN at chain < BN at ring < BNGNT for both armchair and zigzag nanotubes [Fig. S18]. Due to the presence of BN the reflectivity and refractive index decrease depending on doping site [Fig. S17 and Fig. S18]. The reflectivity and refractive index are the highest for pristine systems and the lowest for both armchair and zigzag BNGNTs. From this finding, we can propose that the BNGNT will be of special advantage in optoelectronic devices because optoelectronic devices such as solar cell and LED require materials with low reflectivity. The reflectivity and refractivity spectra with parallel and perpendicular polarizations also show the similar spectral nature. The only

difference is that in the low-energy region, intensity is higher for parallel polarization, but intensity is suppressed due to de-polarization effect in case of perpendicular polarization.

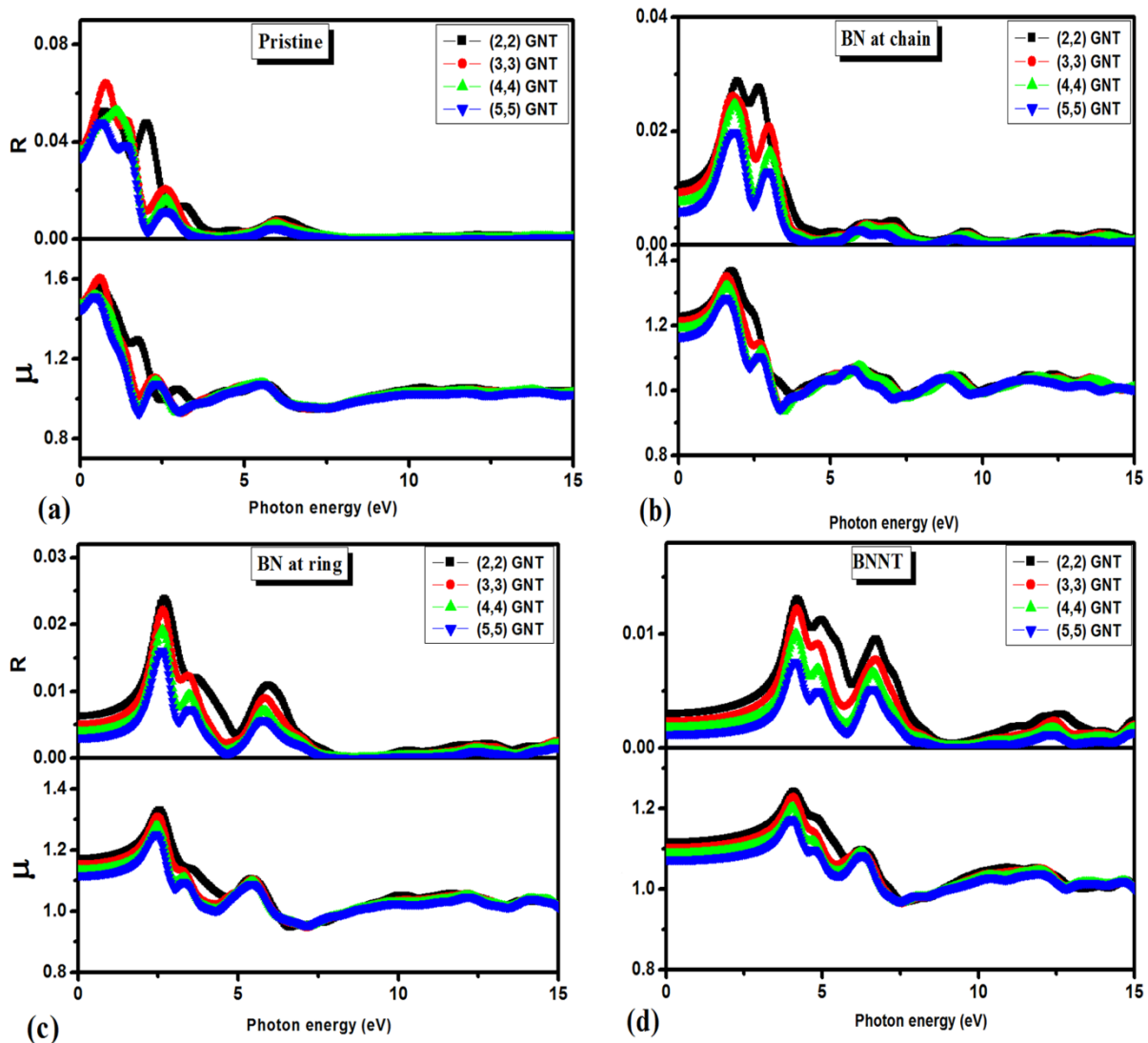


FIG. 14 Diameter dependence of reflectivity $R(\omega)$ and refractivity index $\mu(\omega)$ of zigzag graphyne nanotubes: (a) pristine systems; (b) systems with BN at chain; (c) systems with BN at ring; (d) graphyne like BN nanotubes.

Fig. 15 shows the energy loss spectra of pristine zigzag GNT and their BN derivatives when we consider the average of all directions of propagation. The energy loss spectrum describes the energy dissipated by electron traversing in the material. The peaks in $L(\omega)$ spectra signify features associated with plasma resonance and the frequency corresponding to the plasma resonance represents the plasma frequency, above which the material is a dielectric and below which the system becomes metallic in nature.

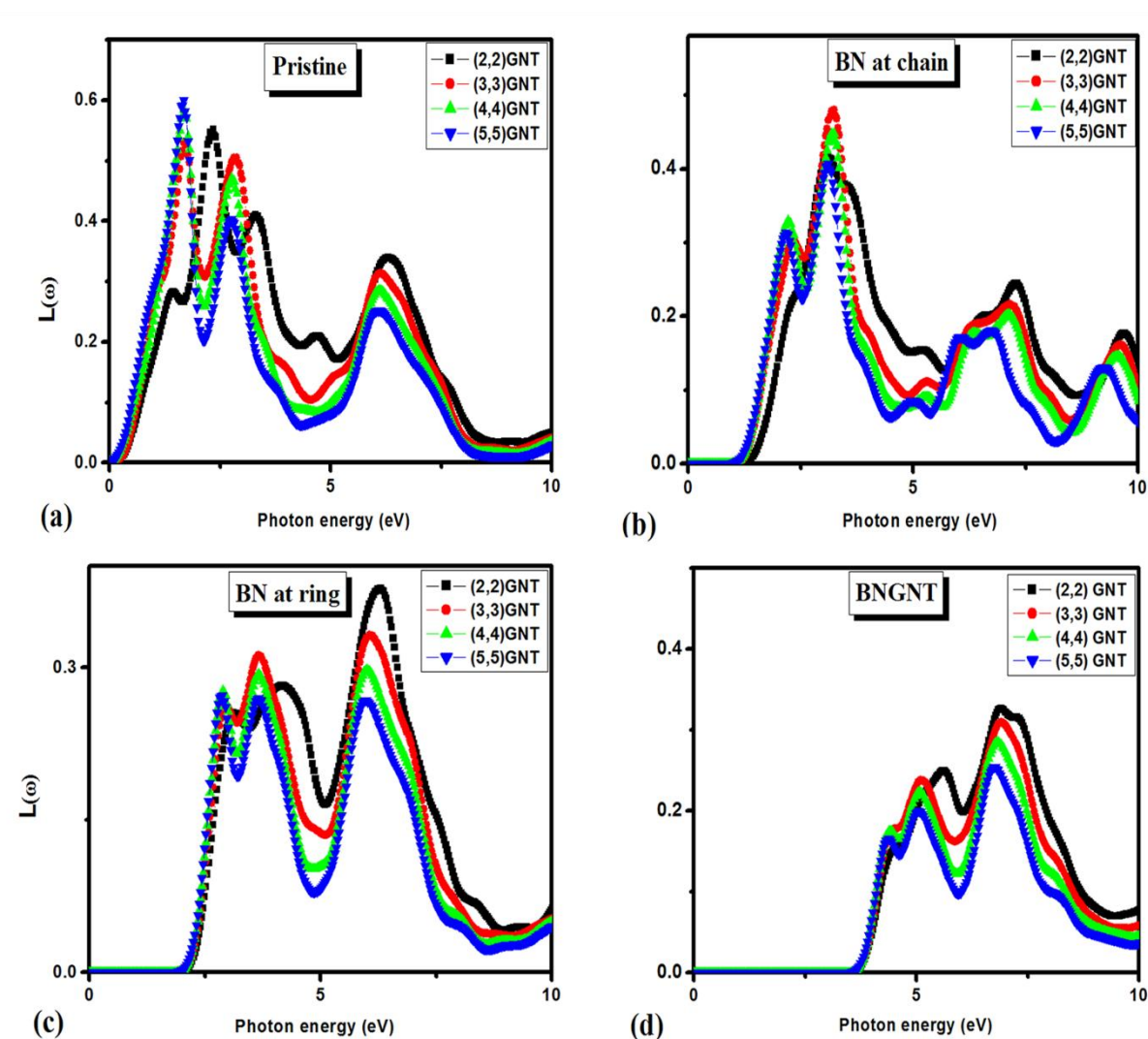


FIG. 15 Diameter dependence of energy loss function $L(\omega)$ of Zigzag graphyne nanotubes: (a) pristine systems; (b) systems with BN at chain; (c) systems with BN at ring; (d) graphyne like BN nanotubes.

One can see from Fig. 15 (a); (b); (c) and (d) that all the structures have the strongest peak at low-energy region and there is a redshift of the strongest peak with increasing diameter. For (2, 2) GNT [Fig.15(a)], below 10.00 eV the strong peak of $L(\omega)$ has been observed which corresponds to plasma frequency at low energy, below the plasma frequency the reflectivity dominates [Fig. 14 (a)] but conductivity is comparatively low [13 (a)] and above this plasma frequency the conductivity dominates but reflectivity becomes zero. Other fundamental structures also mimic the same situations. Due to presence of BN the first strong peak of $L(\omega)$ spectra is shifted towards high energy from infrared to UV region of electromagnetic spectra via visible region. The similar feature has been observed for armchair GNT [Fig. S19].

CONCLUSION

The band gaps of graphyne nanotube depend on diameter and show a damped oscillation with increasing radius. The band gap increases due to the influence of BN and shows the trend: pristine GNT < GNT with BN at chain < GNT with BN at ring < BNGNT. The PDOS analysis reveals that the contribution near the Fermi level is obtained equally from p_x and p_y orbitals of GNTs which is supported by the –COHP study.

Dielectric function shows an overall suppression of intensity for perpendicular polarization over parallel polarization in the low-energy region. As a result, an anisotropy has been found in the low-energy region. The optical properties of GNT are mainly dominated by the tubular geometry rather than its parent planar structure. The presence of BN sweeps the first absorption peak of ϵ_2 spectra towards the UV region of the electromagnetic spectrum obeying the trend: pristine GNT < GNT with BN at chain < GNT with BN at ring < BNGNT. The first peak of absorption spectra, optical conductivity, reflectivity and refractivity are also in conformity with this finding. Absorption spectra analysis suggests that, at the high-energy region, the absorption is mainly contributed by perpendicular polarization while at the low-energy region parallel polarized light is highly absorbed, implying that light polarization can be used for tuning optical response of GNT based optoelectronic devices. An overall diameter dependence of the absorption coefficient, optical conductivity, reflectivity and refractive index has also been found. All these structures exhibit a strong absorption peak in a quite wide UV region and among these structures, only for BNGNT the entire absorption spectrum lies in UV region, which indicates the possibility of its use in UV light protection. Furthermore, due to low dielectric function and large band gap BNGNT may also be considered as a suitable candidate for short-wavelength optoelectronic devices.

ACKNOWLEDGEMENT

The authors wish to acknowledge the assistance of Prof. Paul W. Ayers at McMaster University, and computational resources from Sharcnet and Compute Canada. Dr U Sarkar thanks International Centre for Theoretical Physics, Trieste, Italy for hosting him as a regular associate.

REFERENCES:

- ¹S. Iijima, *Nature* 354, 56 (1991).
- ²K. S. Novoselov, A. K. Geim, S. V. Morozov, D. Jiang, Y. Zhang, S. V. Dubonos, I. V. Grigorieva and A. A. Firsov, *Science* 306, 666 (2004).
- ³D. M. Sun, C. Liu, W. C. Ren and H. M. Cheng, *Small* 9, 1188 (2013).
- ⁴M. F. L. De Volder, S. H. Tawfick, R. H. Baughman and A. J. Hart, *Science* 339, 535 (2013).
- ⁵Q. Zheng and Q. Jiang, *Phys. Rev. Lett.* 88, 045503 (2002).
- ⁶S. B. Legoas, V. R. Coluci, S. F. Braga, P. Z. Coura, S. O. Dantas and D. S. Galvão, *Phys. Rev. Lett.* 90, 055504 (2003).
- ⁷A. Lherbier, S. M. M. Dubois, X. Declerck, S. Roche, Y. M. Niquet and J. C. Charlier, *Phys. Rev. Lett.* 106, 046803 (2011).
- ⁸A. G. Rinzler, J. H. Hafner, P. Nikolaev, L. Lou, S. G. Kim, D. Tomanek, P. Nordlander, D. T. Colbert and R. E. Smalley, *Science* 269, 1550 (1995).
- ⁹S. J. Tans, M. H. Devoret, H. Dal, A. Thess, R. E. Smalley, L. J. Geerligs and C. Dekker, *Nature (London)*, 386, 474 (1997).
- ¹⁰M. Kociak, A. Yu. Kasumov, S. Guéron, B. Reulet, I. I. Khodos, Y. B. Gorbatov, V. T. Volkov, L. Vaccarini and H. Bouchiat, *Phys. Rev. Lett.* 86, 2416 (2001).
- ¹¹S. Mondal, K. Srinivasu, S. K. Ghosh and P. K. Chattaraj, *RSC Adv.* 3, 6991 (2013).
- ¹²A. Chakraborty, S. Giri and P. K. Chattaraj, *Struct Chem.* 22, 823 (2011).
- ¹³R. Das and P. K. Chattaraj, *J. Phys. Chem. A* 116, 3259 (2012).
- ¹⁴R. H. Baughman, H. Eckhardt and M. Kertesz, *J. Chem. Phys.* 87, 6687 (1987).
- ¹⁵Y. Yang and X. Xu, *Comput. Mater. Sci.* 61, 83 (2012).
- ¹⁶J. Chen, J. Xi, D. Wang, and Z. Shuai, *J. Phys. Chem. Lett.* 4, 1443 (2013).
- ¹⁷J. J. Zheng, X. Zhao, Y. L. Zhao, X. F. Gao, *Sci. Rep.* 3, 1271 (2013).
- ¹⁸V. R. Coluci, S. F. Braga, S. B. Legoas, D. S. Galvão and R. H. Baughman, *Phys. Rev. B* 68, 035430 (2003).
- ¹⁹V. R. Coluci, S. F. Braga, S. B. Legoas, D. S. Galvão and R. H. Baughman, *Nanotechnology* 15, S142 (2004).

- ²⁰V. R. Coluci, D. S. Galvão and R. H. Baughman, *J. Chem. Phys.* 121, 3228 (2004).
- ²¹X. M. Wang and S. S. Lu, *J. Phys. Chem. C*, 117, 19740 (2013).
- ²²Y. S. Wang, P. F. Yuan, M. Li, W. F. Jiang, Q. Sun and Y. Jia, *J. Solid State Chem.* 197, 323 (2013).
- ²³R. Majidi and A. R. Karami, *Comput. Mater. Sci.* 97, 227 (2015).
- ²⁴G. Li, Y. Li, H. Liu, Y. Guo, Y. Li and D. Zhu, *Chem. Commun.* 46, 3256 (2010).
- ²⁵J. Kang, J. Li, F. Wu, S. S. Li and J. B. Xia, *J. Phys. Chem. C* 115, 20466 (2011).
- ²⁶J. M. Kehoe, J. H. Kiley, J. J. English, C. A. Johnson, R. C. Petersen and M. M. Haley, *Org. Lett.* 2, 969 (2000).
- ²⁷A. C. Johnson, Y. Lu and M. M. Haley, *Org. Lett.* 9, 3725 (2007).
- ²⁸M. M. Haley, *Pure Appl. Chem.* 80, 519 (2008).
- ²⁹Y. Li, L. Xu, H. Liu and Y. Li, *Chem. Soc. Rev.* 43, 2572 (2014).
- ³⁰J. A. Marsden and M. M. Haley, *J. Org. Chem.* 70, 10213 (2005).
- ³¹G. X. Li, Y. L. Li, X. M. Qian, H. B. Liu, H. W. Lin, N. Chen and Y. J. Li, *J. Phys. Chem. C* 115, 2611 (2011).
- ³²A. Shokri and F. G. Avarsi, *Opt Commun* 304, 143 (2013).
- ³³J. D. Sharma, M. Sharma, N. Kumar and P. K. Ahluwalia, *J. Phys.:Conf. Ser.* 472, 012010 (2013).
- ³⁴S. S. R. K. C Yamijala, A. Bandyopadhyay, and S. K. Pati, *J. Phys. Chem. C* 117, 23295 (2013).
- ³⁵H. Nematian, M. Moradinasab, M. Pourfath, M. Fathipour and H. Kosina, *J. Appl. Phys.* 111, 093512 (2012).
- ³⁶A. Nag, K. Raidongia, K. P. S. S. Hembram, R. Datta, U. V. Waghmare and C. N. R. Rao, *ACS Nano* 4, 1539 (2010).
- ³⁷A. Loiseau, F. Willaime, N. Demoncy, G. Hug and H. Pascard, *Phys. Rev. Lett.* 76, 4737 (1996).
- ³⁸V. V. Pokropivny, A. S. Smolyar and A. V. Pokropivny, *Phys. Solid State*, 49, 591 (2007).
- ³⁹L. Song, L. Ci, H. Lu, P. B. Sorokin, C. Jin, J. Ni, A. G. Kvashnin, D. G. Kvashnin, J. Lou, B. I. Yakobson and P. M. Ajayan, *Nano Lett.* 10, 3209 (2010).

- ⁴⁰X. Hao, S. Dong, W. Fang, J. Zhan, L. Li, X. Xu and M. Jiang, *Inorg. Chem. Commun.* **7**, 592 (2004).
- ⁴¹H. Koga, Y. Nakamura, S. Watanabe and T. Yoshida, *Sci. Technol. Adv. Mater.* **2**, 349 (2001).
- ⁴²Y. N. Xu and W. Y. Ching, *Phys. Rev. B* **44**, 7787 (1991).
- ⁴³K. Watanabe, T. Taniguchi and H. Kanda, *Nature Mater.* **3**, 404 (2004).
- ⁴⁴X. Cao, Y. Li, X. Cheng and Y. Zhang, *Chem. Phys. Lett.* **502**, 217 (2011).
- ⁴⁵A. J. V. Marwitz, E. R. Abbey, J. T. Jenkins, L. V. Zakharov and S. Y. Liu, *Org. Lett.* **9**, 4905 (2007).
- ⁴⁶P. G. Campbell, L. N. Zakharov, D. J. Grant, D. A. Dixon and S. Y. Liu, *J. Am. Chem. Soc.* **132**, 3289 (2010).
- ⁴⁷M. H. Matus, K. D. Anderson, D. M. Camaioni, S. T. Autrey and D. A. Dixon, *J. Phys. Chem. A* **111**, 4411 (2007).
- ⁴⁸M. J. D. Bosdet, C. A. Jaska, W. E. Piers, T. S. Sorensen and M. Parvez, *Org. Lett.* **9**, 1395 (2007).
- ⁴⁹K. H. Oh, D. Lee, M. J. Choo, K. H. Park, S. Jeon, S. H. Hong, J. K. Park and J. W. Choi, *ACS Appl. Mater. Interfaces* **6**, 7751 (2014).
- ⁵⁰W. Mickelson, S. Aloni, W. Q. Han, J. Cumings and A. Zettl, *Science* **300**, 467 (2003).
- ⁵¹D. Golberg, A. Rode, Y. Bando, M. Mitome, E. Gamaly and B. Luther-Davies, *Diam. Relat. Mater.* **12**, 1269 (2003).
- ⁵²A. Nishiwaki, T. Oku, I. Narita, *Sci. Tech. Adv. Mater.* **5**, 629 (2004).
- ⁵³F. D. Angelis, S. Fantacci and R. Gebauer, *J. Phys. Chem. Lett.* **2**, 813 (2011).
- ⁵⁴O. B. Malcioğlu, A. Calzolari, R. Gebauer, D. Varsano and S. Baroni, *J. Am. Chem. Soc.* **133**, 15425 (2011).
- ⁵⁵J. M. Soler, E. Artacho, J. D. Gale, A. García, J. Junquera, P. Ordejón and D. S. Portal, *J. Phys. Condens. Matter* **14**, 2745 (2002).
- ⁵⁶N. Troullier and J. Martins, *Solid State Commun.* **74**, 613 (1990).
- ⁵⁷X. Blase, A. Rubio, S. G. Louie and M. L. Cohen, *Euro. Phys. Lett.* **28**, 335 (1994).
- ⁵⁸N. G. Chopra, R. J. Luyken, K. Cherrey, V. H. Crespi, M. L. Cohen, S. G. Louie and A. Zettl, *Science* **269**, 966 (1995).

- ⁵⁹N. B. Singh, B. Bhattacharya and U. Sarkar, *Struct. Chem.* 25, 1695 (2014).
- ⁶⁰M. L. Cohen and A. Zettl, *Phys. Today X*, 34 (2010).
- ⁶¹D. A. Britz and A. N. Khlobystov, *Chem. Soc. Rev.* 35, 637 (2006).
- ⁶²B. Bhattacharya, N. B. Singh and U. Sarkar, *Int. J. Quant. Chem.* 115, 820 (2015).
- ⁶³T. M. Gilbert, *Organometallics*, 19, 1160 (2000).
- ⁶⁴M. J. D. Bosdet and W. E. Piers, *Can. J. Chem.* 87, 8 (2009).
- ⁶⁵P. Paetzold, *Pure Appl. Chem.* 63, 345 (1991).
- ⁶⁶M. H. Matus, S. Y. Liu, and D. A. Dixon, *J. Phys. Chem. A* 114, 2644 (2010).
- ⁶⁷D. Grant and D. A. Dixon, *J. Phys. Chem. A* 110, 12955 (2006).
- ⁶⁸D. A. Dixon and M. Gutowski, *J. Phys. Chem. A* 109, 5129 (2005).
- ⁶⁹M. H. Matus, D. J. Grant, M. T. Nguyen, and D. A. Dixon, *J. Phys. Chem. C* 113, 16553 (2009).
- ⁷⁰Z. Gan, D. J. Grant, R. J. Harrison and D. A. Dixon, *J. Chem. Phys.* 125, 124311 (2006).
- ⁷¹M. T. Nguyen, M. H. Matus, W. A. Lester, Jr, and D. A. Dixon, *J. Phys. Chem. A* 112, 2083 (2008).
- ⁷²M. Topsakal, E. Akturk, and S. Ciraci, *Phys. Rev. B* 79, 115442 (2009).
- ⁷³R. J. Boyd, S. C. Choi and C. C. Hale, *Chem. Phys. Lett.* 112, 136 (1984).
- ⁷⁴A. J. V. Marwitz, M. H. Matus, L. N. Zakharov, D. A. Dixon, S. Y. Liu, *Angew. Chem. Int. Ed.* 48, 973 (2009).
- ⁷⁵X. M. Wang and S. S. Lu, *J. Phys. Chem. C* 117, 19740 (2013).
- ⁷⁶J. Kang, J. Li, F. Wu, S. S. Li and J. B. Xia, *J. Phys. Chem. C* 115, 20466 (2011).
- ⁷⁷H. X. Jie, T. Jie, B. H. Xia, Z. H. Yu, Z. M. Wen, *Chin. Sci. Bull.* 57, 3080(2012).
- ⁷⁸G. Y. Guo, K. C. Chu, D. Wang and C. Duan, *Phys. Rev. B* 69, 205416 (2004).
- ⁷⁹L. M. Yang and R. Pushpa, *J. Mater. Chem. C* 2, 2404 (2014).